

Ion-surface interactions in the electron-stimulated desorption of Cl^+ from $\text{Cl}_2/\text{Si}(111)\text{-}7\times 7$

W. C. Simpson and J. A. Yarmoff*

*Department of Physics, University of California, Riverside, California 92521
and Material Sciences Division, Lawrence Berkeley Laboratory, Berkeley, California 94720*

(Received 17 February 1995; revised manuscript received 24 March 1995)

Cl^+ electron-stimulated desorption energy and angular distributions are collected from $\text{Si}(111)\text{-}7\times 7$ surfaces exposed to Cl_2 . The results of these measurements are fitted to a model that accounts for variations in the surface work function, ion-surface image-charge interactions, and ion neutralization. From the fits, the strength of the image-charge interaction and the angular dependence of the neutralization are determined. The ideas presented here concerning the motion of ions in the vicinity of a surface are generally valid for all ion-surface interactions.

I. INTRODUCTION

The proper interpretation of many experimental techniques requires a basic understanding of how the motion of an ion near a solid surface is perturbed by the presence of the surface. In essence, one needs to know how the energy and trajectory of an ion measured far from a given surface are related to that same ion's energy and trajectory near the surface. This is not only a basic physics problem, but it also has great importance to many in the surface science community who use ions to study or alter surfaces. Electric fields, ion-surface image-charge interactions and neutralization can, and do, drastically alter the energy and angular distributions of ions, so that what is measured may not directly reflect what is happening near the surface. These effects must therefore be considered in order to understand the physics behind such varied techniques as low-energy ion scattering, low-energy ion deposition, sputtering, electron- and photon-stimulated desorption, secondary-ion-mass spectrometry, and metastable ion quenching.

As the ion kinetic energy decreases, the relative effects of these ion-surface interactions are greatly enhanced, and cannot safely be neglected for processes in which the energy of the ion is only a few eV, as in the case of stimulated desorption. The problem of how to remove the distorting effects of ion-surface image-charge interactions from stimulated desorption ion energy and angular distributions has been looked at in the past,¹ and a theoretical framework exists for relating the measured ion flux to the ion flux that is initially formed at the surface, ignoring neutralization. The neutralization of ions by a surface has also been investigated, both experimentally and theoretically, providing a means to quantify the effects of neutralization on the total ion yield.^{2,3} In this investigation, the experimental results of a stimulated desorption experiment are fit to a model based on these earlier studies, which combines these effects in order to generate a more complete picture of the interaction of ions with a surface.

Specifically, the interaction of Cl^+ ions with a chlorinated $\text{Si}(111)\text{-}7\times 7$ surface is studied, using electron-stimulated desorption (ESD) to generate the ions near the

surface. The approach taken is to use the ions generated via ESD to investigate ion-surface interactions rather than to study the initial excitations that lead to stimulated desorption, which are already understood for the Cl_2/Si system.⁴⁻⁶ In this study, secondary electron cutoffs and Cl^+ ion energy and angular distributions (IEAD's) are collected as a function of increasing chlorination. The results of these measurements are fit to a model that accounts for alternations of the initial IEAD due to work-function differences between the surface and the detector, image-charge interactions, and neutralization. Several aspects of the model are general enough that they can be applied to any ion-surface interaction study.

The $\text{Cl}_2/\text{Si}(111)\text{-}7\times 7$ system was chosen for several reasons. First, it has a simple geometry, in that the Cl^+ ions are emitted primarily normal to the surface. Second, for this system, the trajectory-altering effects of the image-charge interaction are expected to be quite large because the initial kinetic energy of the Cl^+ ions is comparable to the strength of the image-charge interaction. Third, the initial excitations that lead to Cl^+ -stimulated desorption from Si are well known.⁴⁻⁶ Finally, the measured kinetic energy of the Cl^+ ions is only ~ 1 eV, low enough that the ion kinetic-energy distribution (IKED) has a cutoff due to the vacuum level of the surface passing through the IKED. The observation of such an ion cutoff is rare, and allows the position of the positive ion vacuum level to be followed explicitly throughout the experiment.

II. EXPERIMENTAL PROCEDURE

All measurements were carried out in an ultrahigh vacuum (UHV) chamber equipped with an electron gun, a quadrupole mass spectrometer (QMS), a hemispherical electrostatic energy analyzer (ESA), and a four-grid retarding field analyzer (RFA) low-energy electron-diffraction/Auger-electron spectroscopy (LEED/AES) system. Single-crystal $\text{Si}(111)$ samples (n type, $\sim 1 \Omega \text{ cm}$, $\pm 0.25^\circ$) were mounted on a manipulator which rotates through an axis parallel to the surface, so that ions and electrons can be collected at a variety of polar emission

angles relative to the surface normal. All off-normal measurements were made along a single arbitrary azimuth, so that no claim is made regarding the dependence of the reported quantities on azimuthal angle. However, since the $\text{Cl}_2/\text{Si}(111)\text{-}7\times 7$ system primarily exhibits normal emission of Cl^+ , any azimuthal variations in the ion yield are expected to be small. The Si samples were cleaned by resistively heating them to $\sim 1050^\circ\text{C}$. Sample cleanliness and crystallinity were checked by AES and by the existence of a sharp 7×7 LEED pattern, respectively.

Samples were exposed *in situ* to Cl_2 produced by an AgCl solid-state electrochemical cell.⁷ In order to ascertain the Cl coverage after each exposure, a Cl/Si AES ratio was determined by collecting first-derivative AES spectra with a 3-keV electron beam and taking the ratio of the Cl(LMM) to Si(LMM) peak-to-peak intensities. This measured Cl/Si AES ratio is proportional to the Cl coverage, granted that no multilayer growth occurs. To convert to Cl coverage, the Cl/Si AES ratio of 1.1 found in this study for a Cl-saturated surface is assumed to correspond to the saturation coverage of $\Theta_{\text{Cl}}=1.9$ ML determined via photoelectron spectroscopy.^{4,8} Due to small differences in the reported saturation coverage, the Cl coverage calibration has an estimated uncertainty of $\sim 10\%$. However, any inaccuracies in the reported coverages due to the method of calibration will not affect the conclusions of this work, since the Cl coverage is used as a convenient label (except where noted).

Care was taken to minimize electron-beam damage during the AES and cutoff measurements. A 300-eV electron beam was used to excite both the ESD Cl^+ ions and the secondary electrons for the cutoff measurements. To limit beam damage during the cutoff measurements, the total current on the sample was kept below ~ 10 nA, with a typical spot size of about 1 mm in diameter and a typical collection time of ~ 600 s. In the collection of the AES spectra, the total current on the sample was typically ~ 1 μA , in a spot size of about 2 mm in diameter. Because the electron beam used to collect AES spectra had a higher energy and current, it was more likely to cause beam damage. Therefore, AES measurements were always carried out after the cutoff measurements, and were collected quickly (typically in ~ 200 s) to prevent the desorption of an appreciable amount of Cl from the surface during the measurements.

In order to have the angle and energy resolution required for this study, an ESA was used instead of a RFA apparatus, which is more commonly used to study ESD ion angular distributions (ESDIAD).^{9,10} In addition to having higher resolution, ESA's generally distort the ESDIAD pattern much less than a RFA, since the analyzer-to-sample distance can be increased and since it is not necessary to apply a compressive field between the sample and analyzer in order to collect the ESDIAD pattern. The Cl^+ ion kinetic-energy distributions were measured, using the ESA, with a total-energy resolution of 0.50 eV and an angular acceptance of $\sim 4^\circ$. The secondary electron cutoffs were also collected using the ESA, with the same resolution and angular acceptance, by simply reversing the polarity of the appropriate elements in the analyzer. The sample was biased +10 V relative to

the analyzer when measuring ions, and -10 V when measuring electrons, so that the vacuum level of the analyzer was well below that of the sample. This ensures that the vacuum level of the analyzer itself does not directly affect the shape of the cutoffs.

Due to the high ESD cross section of fluorine, the possibility of F^+ contamination is always a concern in ESD experiments, especially from Si substrates, which exhibit F^+ ESD even when no F has been explicitly introduced to the surface.^{11,12} Because of this, two steps were taken to identify the ESD ions detected in this experiment. First, the ESD ions were identified with the QMS, by turning its ionizer off and measuring the mass distribution of ions ejected normal to the surface. Second, since F^+ ions desorbing from Si surfaces have a higher kinetic energy than Cl^+ ions, the contribution to the IKED's arising from F^+ is easily identified.⁴ The fact that only trace amounts of F^+ were ever detected with QMS, and that no evidence for F^+ ions was found in any of the IKED's, verifies that Cl^+ is the primary desorption product.

III. RESULTS AND MODEL

In order to properly interpret the Cl^+ IEAD's collected in this study, the distorting effects of the surface on the IEAD's are accounted for with a model that focuses on three aspects of the ion-surface interaction. First, since the sample is biased relative to the detector, and since the detector and the sample do not necessarily have the same work function, there are weak external electric fields present during the measurements which act primarily to offset the measured energies. Second, the angular distribution and the initial energies of the ions are altered due to the image-charge interaction between the escaping ions and the surface. Finally, neutralization preferentially removes a large percentage of the Cl^+ signal at off-normal angles. All these effects must be considered in order to determine the initial energy and angular distribution of the ions near the surface.

A. Work-function-induced shifts

Secondary electron cutoffs and Cl^+ IKED's were collected from a $\text{Si}(111)\text{-}7\times 7$ surface following exposure to increasing amounts of Cl_2 . The secondary electron cutoffs shift toward higher kinetic energy with increasing Cl coverage, indicating an increase in the work function. In contrast, the Cl^+ IKED's are found to shift toward lower kinetic energy, as well as to broaden and change shape somewhat, with increasing coverage. The shift of the IKED's with increasing work function complicates their analysis, and needs to be removed in order to follow their evolution with increasing Cl coverage.

This work-function-induced shift is removed by displaying the IKED's with respect to the vacuum level of the sample, rather than that of the analyzer. In this study, the position of the positive ion vacuum level, relative to the sample, is followed throughout the experiment by tracking the position of the IKED cutoff. If the IKED's did not exhibit a cutoff, it would be impossible to

determine experimentally how to properly align them, since they change shape as well as shift in energy. Note that it is rare to observe such a cutoff in ESD IKED's, since most ESD ions have kinetic energies that are sufficiently high that there is no measurable ion intensity near the cutoff. As a result, in many stimulated desorption studies, IKED's are left uncorrected or are arbitrarily offset to align a particular feature, such as the leading edge.^{4,12-14} However, by comparing the offset of the IKED to changes in the surface work function, as is done in the present study, the validity of a simple model which accounts for these IKED energy offsets is confirmed, thereby eliminating the problem. With the use of this model, the true zero for the ion kinetic energy can be determined for the majority of cases in which a cutoff is not observed.

The magnitude of the energy shift in the IKED cutoffs follows the change in the work function, as is seen in Fig. 1, which shows the shift in kinetic energy relative to the analyzer vacuum level of both the secondary electron and Cl^+ IKED cutoffs as a function of Cl coverage. The change in the work function with Cl coverage was determined by aligning the leading edge of the secondary electron cutoff with that of a reference spectrum collected from a clean surface. Since the Cl^+ IKED's extend down to zero kinetic energy, their cutoffs were determined by first numerically removing the Gaussian broadening due to the finite analyzer resolution, and then finding the lowest energy with measurable ion intensity and assigning it to zero. The magnitude of the IKED shifts with Cl coverage were then determined by comparison to the cutoff measured for the lowest exposure.

There is a simple reason to expect the energy shift in the IKED cutoffs to be equal and opposite to the change

in the work function. For an electron emitted from a sample of work function ϕ_{sample} that is biased with a voltage V_s relative to an analyzer of work function ϕ_{an} , the relationship between the observed kinetic energy of the electron and its kinetic energy relative to the vacuum level of the sample is

$$E_{\text{kin}}^{\text{an}} = E_{\text{kin}}^{\text{sample}} - eV_s - e(\phi_{\text{an}} - \phi_{\text{sample}}). \quad (1)$$

The difference in the two kinetic energies arises from the macroscopic electric field generated between the sample and analyzer by the bias voltage and work-function difference. This field acts in an equal and opposite manner on positive ions,¹⁵ so that for a positive ion

$$E_{\text{kin}}^{\text{an}} = E_{\text{kin}}^{\text{sample}} + eV_s + e(\phi_{\text{an}} - \phi_{\text{sample}}). \quad (2)$$

Therefore, an increase in the work function of the sample will have an equal but opposite effect on the kinetic energies of electrons and positive ions measured at the analyzer.

The solid line in Fig. 1 represents a fit to the expected work-function shift vs coverage, derived from a model for work-function changes that arise from a buildup of screened dipoles on a surface.¹⁶ The equation to which the data are fit is

$$e\Delta\phi = -4\pi(epn_{\text{dip}})/(1 + 9\alpha n_{\text{dip}}^{3/2}), \quad (3)$$

where n_{dip} is the density of Cl—Si bonds on the surface, and p (the Cl-Si dipole strength) and α (the polarizability of the dipoles) are determined from the fit. The best fit to the data gives $p = 4 \times 10^{-30}$ C m and $\alpha = 2 \times 10^{-39}$ C² m/N. For comparison, some tabulated values of p for Si-Cl compounds are 2.9×10^{-30} C m for SiHCl_3 , 3.9×10^{-30} C m for SiH_2Cl_2 , and 4.3×10^{-30} C m for SiH_3Cl .¹⁷ Note that the values of p and α reported here depend directly on the Cl coverage calibration, and therefore have some small uncertainty due to the method of calibration. The dashed line in Fig. 1 is the reflection of the solid line about zero, which is included in the figure to illustrate how the IKED cutoff shifts mirror those of the work function.

These results show two things. One, the work function shift vs Cl coverage is consistent with the buildup of a layer of Si-Cl dipoles on the surface. Two, the low-energy cutoffs for electrons and positive ions are effected in an equal but opposite manner by changes in the sample work function, confirming the ideas behind Eqs. (1) and (2). Thus if both a secondary electron cutoff and an IKED are collected from a given surface, the sample work function determined from the secondary electron cutoff can be used to find the correct energy offset for the IKED, so that it can be reported relative to the vacuum level of the sample. This technique is especially useful in the majority of cases for which there is no low-energy cutoff in the IKED.

Figure 2 shows the Cl^+ IKED's for various Cl coverages, after correcting for the applied bias voltage and work-function difference. With these corrections made, the IKED's are all plotted on the same energy axis, so that their evolution with increasing Cl coverage can be examined. The mean kinetic energy at low coverages is

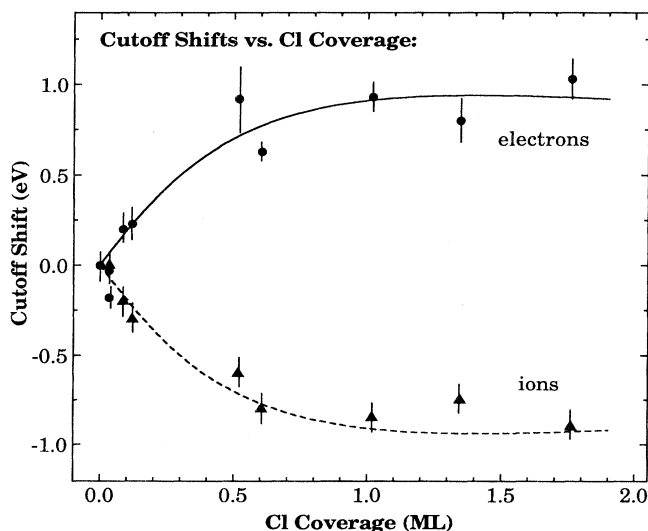


FIG. 1. Measured shifts of the secondary electron cutoffs (circles) and Cl^+ kinetic-energy distribution cutoffs (triangles) with increasing Cl coverage. The solid line represents a fit to a screened dipole model (see text). The dashed line is a reflection of the solid line about zero.

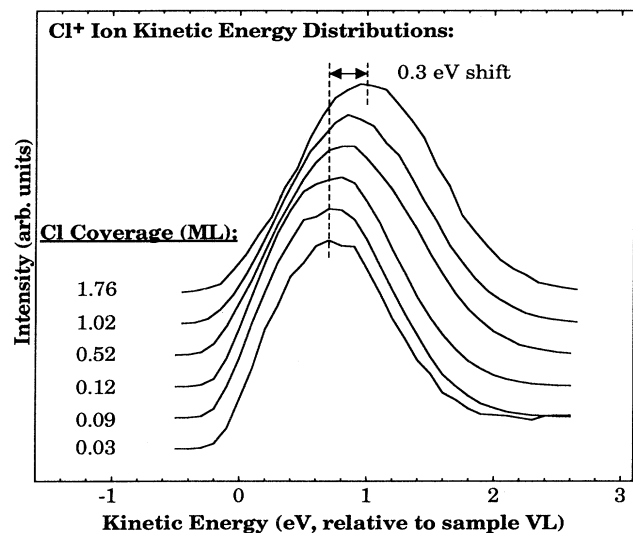


FIG. 2. Cl^+ kinetic-energy distributions collected normal to the surface from $\text{Si}(111)\text{-}7\times 7$ surfaces exposed to various amounts of Cl_2 . The data are labeled with their corresponding Cl coverages. Energies are reported with respect to the vacuum level (VL) of the sample.

~ 0.7 eV. As indicated in the figure, the IKED's shift ~ 0.3 eV toward higher kinetic energy at the highest Cl coverages. There are many factors, involving both the initial and final states, that contribute to the kinetic energy of the desorbing ions, and hence there are many potential origins for the observed shift with increasing Cl coverage. One initial-state effect that could shift the observed IKED to higher kinetic energy is an increase in the repulsive $\text{Si}^+\text{-Cl}^+$ interaction that is responsible for Cl^+ desorption.⁵ That is, since the formation of an electronegative Cl adlayer removes some valence electronic charge from the vicinity of the outermost Si atoms, the system's capacity to screen out a hole localized on a surface Si atom is decreased, thereby increasing the repulsive $\text{Si}^+\text{-Cl}^+$ interaction during Cl^+ desorption. A final-state effect that could shift the observed kinetic-energy distribution is an increase in the neutralization probability for the lowest-energy Cl^+ ions. Another is that chlorination of the surface might reduce the strength of the image-charge interaction felt by a desorbing ion, either by changing the initial ion-to-image-plane distance or by changing the effective dielectric constant of the surface. Unfortunately, there is not enough information present in the data to distinguish which of these effects causes the observed IKED shift with increasing Cl coverage.

B. Image-charge interactions

In ESD from the $\text{Cl}_2/\text{Si}(111)\text{-}7\times 7$ system, Cl^+ emission is observed only within a narrow lobe centered about the surface normal direction, as is shown in Fig. 3. To generate the data shown in Fig. 3, full IKED spectra were collected at 10° intervals along the same arbitrary azimuth and then integrated. The integrated IKED in-

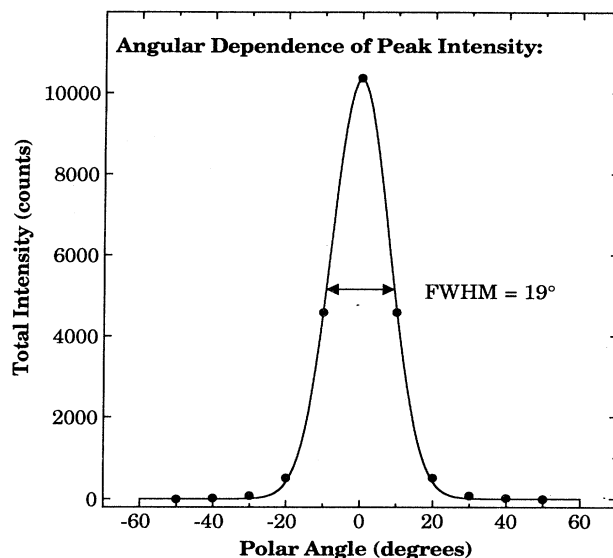


FIG. 3. Total Cl^+ ESD yield vs the polar angle of collection, from a Cl_2 -covered $\text{Si}(111)\text{-}7\times 7$ surface. The data are shown as filled circles. The solid line represents a Gaussian fit to the data.

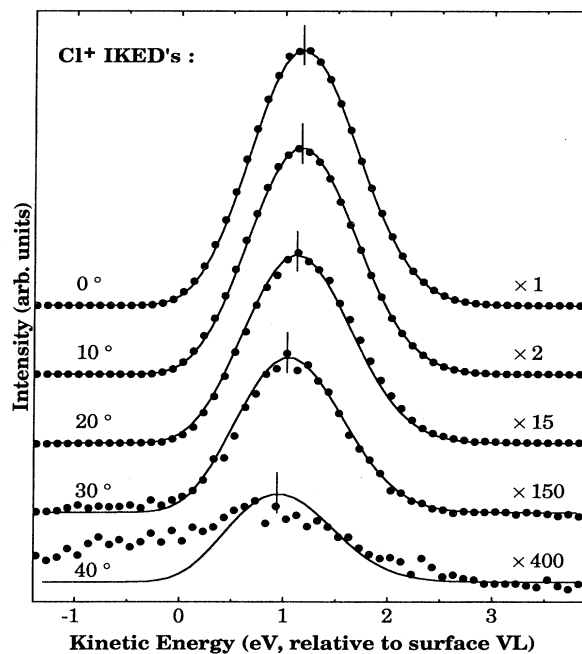


FIG. 4. Cl^+ kinetic-energy distributions collected along the same azimuth, but at different polar angles, from a Cl_2 -covered $\text{Si}(111)$ surface. The data (circles) are labeled with the polar angle at which they were collected, and are scaled to fit in the same figure, with the scaling factors noted. The curves drawn through the data represent fits to a model (see text). For each angle, a short vertical line has been drawn to indicate the location of the peak center.

tensity was then plotted as a function of the angle of orientation of the ESA with respect to the surface normal. The solid line in Fig. 3 represents a Gaussian fit to the data, with a best-fit full width at half maximum (FWHM) of 19° . Note that this value is only accurate to within about 1° due to the finite angular acceptance of the detector as well as uncertainties in angular alignment.

The IKED's used to generate Fig. 3 are shown in Fig. 4. The filled circles are the raw data, scaled to fit on the same figure (with the scaling factors indicated), and the solid curves represent theoretical fits to the data, which are explained in detail below. There are several trends in the data that are accounted for in the fits. First, the position of the IKED peak maximum shifts toward lower kinetic energy as the angle of emission is increased. This can be seen in Fig. 4, in which the locations of peak maxima are indicated with vertical lines. The angular dependence of this shift depends sensitively on the energetics of the desorption process. Second, the total IKED intensity is attenuated with increasing angle, as can be seen perhaps more clearly in Fig. 3. This is a result of a combination of recapture and neutralization. Finally, the overall shape of the IKED's is nearly Gaussian, with a width that is essentially independent of the angle, suggesting that the initial IKED is likely to be Gaussian.

In fact, a Gaussian distribution of energies and desorption directions for ESD ions, as they are initially formed near a surface, has been shown to be a quite reasonable model.^{18,19} Therefore, it is assumed that the initial desorbing ion flux is of the form

$$I_0(E_0, \theta_0) \propto \exp \left[- \frac{\left(\frac{E_0 - \bar{E}_0}{(\Delta E_0/2\sqrt{\ln 2})} \right)^2}{\left(\frac{\theta_0 - \bar{\theta}_0}{(\Delta \theta_0/2\sqrt{\ln 2})} \right)^2} \right], \quad (4)$$

$$I(E, \theta) = A_0 \exp \left[- \frac{\left(\frac{E + W - \bar{E}_0}{(\Delta E_0/2\sqrt{\ln 2})} \right)^2}{\left(\frac{\sin^{-1} \left[\sin \theta \left(\frac{E}{E + W} \right)^{1/2} \right] - \bar{\theta}_0}{(\Delta \theta_0/2\sqrt{\ln 2})} \right)^2} \right] J(E, \theta), \quad (7)$$

where $J(E, \theta)$ is the Jacobian of the transformation from (E_0, θ_0) to (E, θ) ,

$$J(E, \theta) = \frac{E \cos \theta}{\sqrt{(E + W)(E \cos^2 \theta + W)}}, \quad (8)$$

and A_0 is a proportionality constant. Ions with initial kinetic energy E_0 , that have an initial desorption angle greater than a certain critical angle $\theta_c(E_0)$, do not have enough kinetic energy normal to the surface, and are recaptured by the ion-surface image potential. This critical angle for recapture is given by

where ΔE_0 is the FWHM of the initial desorption kinetic-energy distribution, which is centered about the mean value \bar{E}_0 , and $\Delta \theta_0$ is the FWHM of the initial distribution of desorption angles, which is centered about the mean value $\bar{\theta}_0$. Note that no explicit dependence on the azimuthal angle is included in this analysis, and that factors of $2\sqrt{\ln 2}$ have been introduced so that each width is a FWHM.

Once an ion is formed, there is an attractive image force between it and the surface, directed along the surface normal. The image interaction retards the ion's velocity normal to the surface, having two effects. One, the measured energy of the ion far from the surface, E , is less than the initial kinetic energy E_0 by an amount equal to the initial image-charge interaction strength W . In fact, if E_0 is less than W , the ion will not escape the surface. Two, the final emission angle of the ion far from the surface, θ , is greater than or equal to the initial emission angle near the surface, θ_0 , with the degree of deviation depending on the ion's kinetic energy. Thus, although the initial IKED may be highly symmetric, the final IKED will not necessarily reflect this symmetry due to the distorting effects of the image-charge interaction. A relationship between the initial and final energies, angles and ion fluxes, as given by Miskovic, Vukanic, and Madey,¹ is

$$E_0 = E + W, \quad (5)$$

$$\theta_0 = \sin^{-1} \left[\sin \theta \left(\frac{E}{E + W} \right)^{1/2} \right], \quad (6)$$

and

$$\theta_c(E_0) = \cos^{-1} \left[\left(\frac{W}{E_0} \right)^{1/2} \right]. \quad (9)$$

In addition, no ion will be detected with a kinetic energy below that which corresponds to the vacuum level of the surface. If the initial IKED has a measurable intensity near this ion vacuum level, a cutoff will be observed, as is the case for Cl^+ ESD from $\text{Cl}_2/\text{Si}(111)$ - 7×7 .

Because the data shown in Fig. 4 are somewhat broad and structureless, there is no unique set of parameters that gives a definitive best match to the data. Therefore, in order to fit the measured IKED's with physically reasonable parameters, estimates for \bar{E}_0 , ΔE_0 , $\bar{\theta}_0$, $\Delta \theta_0$,

and W were first made. From these estimates, a model IKED was generated numerically for each detection angle θ , using Eqs. (5)–(8). Each model IKED was then numerically convolved with a Gaussian to fold in broadening effects due to the finite detector resolution, and the broadened IKED's were compared to the measured IKED's, matching the line shapes but not the overall intensities, which are reduced by neutralization (as discussed below). Variations of the parameters were then considered, in order to find the best overall match between the model IKED's and the measured IKED's.

An estimate for the image-charge interaction strength W was obtained using the equation $W = (e^2/4\pi\epsilon_0)(1/4s)(\kappa-1)/(\kappa+1)$, where s is the ion-to-image-plane separation at the point at which the ion is formed.²⁰ In the case of chlorinated Si, the location of the image plane is somewhat ambiguous, since the substrate is not metallic. A reasonable compromise is to place the image plane somewhere between the outermost surface Si atoms and the Cl adlayer, because some valence electronic charge extends out beyond the Si atoms, either in the dangling bonds of unreacted Si atoms or in the Cl adatoms situated above reacted Si atoms. Assuming that the image plane is located about halfway between the topmost layer of Si atoms and the Cl adlayer, s is estimated to be ~ 1 Å, or roughly half the Cl–Si bond length.²¹ With a dielectric constant for Si of $\kappa = 11.9$,¹⁷ this corresponds to $W \sim 3$ eV. The parameters \bar{E}_0 , ΔE_0 , $\bar{\theta}_0$, and $\Delta\theta_0$ were estimated directly from the measured IKED's. The FWHM of the measured IKED's is about 1 eV, and the mean kinetic energy of the measured IKED's is also about 1 eV at the Cl coverage used

to generate Figs. 3 and 4. With $W \sim 3$ eV and a mean measured kinetic energy of ~ 1 eV, \bar{E}_0 is about 4 eV. Also, as shown in Fig. 3, the angular distribution is centered about $\theta = 0$, so that $\bar{\theta}_0 = 0$. Since the FWHM of the angular distribution is 19° , a reasonable estimate for the FWHM of the angular distribution near the surface is $\sim 20^\circ$. Finally, as determined from a measurement of the secondary electron cutoff, there is a 1.53-eV offset correction to the kinetic energy due to a difference in the work functions of the sample and detector at this coverage.

Although these estimates for \bar{E}_0 , ΔE_0 , $\bar{\theta}_0$, $\Delta\theta_0$, and W give a reasonable fit to the data, the best fit is obtained with $W = 3.6$ eV, $\bar{E}_0 = 4.6$ eV, $\Delta E_0 = 1.2$ eV, and $\Delta\theta_0 = 25^\circ$. These best-fit numbers, in combination with Eq. (4), give a reasonable reconstruction of the initial IEAD from the data. They also contain information about the image-charge interaction. An initial image-charge interaction strength of $W = 3.6$ eV places the image plane about 1.2 Å above the topmost Si layer. Also, for ions desorbing with the mean initial kinetic energy of $\bar{E}_0 = 4.6$ eV, the critical angle for recapture is 28° . There is a wide spread in the initial kinetic energies, however, leading to a spread in the critical angle, so that an ion desorbing with energy $\bar{E}_0 + \Delta E_0/2$ has a critical angle of 34° , whereas one with energy $\bar{E}_0 - \Delta E_0/2$ has a critical angle of only 18° . Thus, only the highest kinetic-energy ions escape the surface if their initial desorption θ_0 angle is greater than about $30^\circ - 35^\circ$.

C. Neutralization

The effects of neutralization are ignored in the above model. Therefore, the ion yield found using Eqs. (7) and (8) is expected to be proportional to the yield of ions from the surface prior to any neutralization. Since the intensity of the measured IKED's is attenuated by neutralization, an estimate of the degree of ion neutralization can be found by taking the ratio of the measured ion yield to the predicted yield. A plot of the angular dependence of this ratio, which is proportional to the ion survival probability, is given in Fig. 5. As is shown clearly in the figure, there is a strong angular dependence of the ion survival probability, which acts to remove ion intensity preferentially from the off-normal directions.

To quantify the angular dependence of neutralization, a simple model is used to fit the data shown in Fig. 5, based on Hagstrum's ideas about the neutralization of noble gas ions near a metal surface.³ The neutralization of Cl^+ ions and positive noble gas ions are expected to be similar, since Cl, like noble gas atoms, has a large ionization potential and therefore undergoes the same irreversible Auger-like neutralization process. In this model, if an ion is moving near a surface along a trajectory with polar angle θ_0 , the probability that it will survive the encounter as a positive ion has the form

$$P^+(\theta_0) = \exp \left[- \left[\frac{V}{v_0} \right] \left[\frac{1}{\cos\theta_0} \right] \right]. \quad (10)$$

V is related to the neutralization rate $R(z)$, where z is the distance between the ion and the image plane, by

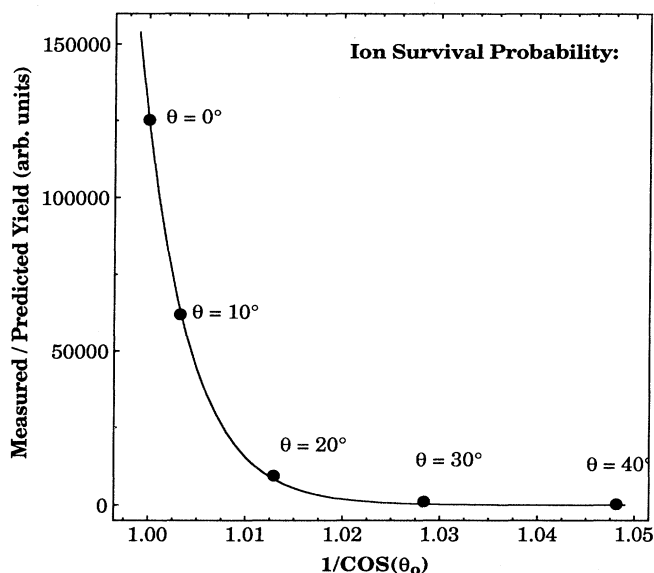


FIG. 5. The ratio of the measured total Cl^+ yield to the Cl^+ yield predicted from the model, which is proportional to the ion survival probability, plotted with respect to $1/\cos\theta_0$. Each data point (filled circle) is labeled with the corresponding angle of collection θ . The solid line represents a fit to a decay exponential, corresponding to a Hagstrum-type neutralization process.

$$V = \int_s^\infty R(z) dz, \quad (11)$$

where, again, s is the distance above the image plane at which the ion was initially formed. In this model, the initial velocity of the ion, v_0 , is calculated from the mean initial kinetic energy using the relation

$$\bar{E}_0 = \frac{1}{2} m v_0^2. \quad (12)$$

The use of this monoenergetic approximation allows the effects of neutralization on the IKED line shape, for a given angle, to be factored out from those due to the image-charge interaction. Although the energy dependence of neutralization is averaged out, the angular dependence of the ion survival probability is still preserved. The monoenergetic approximation works best in cases where the ions have a high kinetic energy near the surface, or have a very narrow spread in energies, and is thus considered a reasonable assumption for this study since $(\Delta E_0 / \bar{E}_0) \sim 0.15$.

The ratio of the measured ion yield to the predicted total yield is shown in Fig. 5. The data are labeled with their corresponding detection angle θ , but are plotted vs $1/\cos\theta_0$, where θ_0 was calculated from θ using Eqs. (5) and (6) by replacing E_0 with \bar{E}_0 . As is seen in the figure, the ion survival rate drops precipitously with the angle, so that ions emitted 20° from normal are neutralized over 100 times more efficiently than those emitted normal to the surface. Included in the figure is a decaying exponential fit to the data, as is expected for Hagstrum-type neutralization, with a best-fit value of $(V/v_0) = 208$. A mean initial kinetic energy $\bar{E}_0 = 4.6$ eV corresponds, via Eq. (12), to a mean initial velocity of $v_0 = 5000$ m/s. Thus, with $(V/v_0) = 208$, it is found that $V = 1.04 \times 10^6$ m/s.

For a nonlocal irreversible neutralization process, $R(z)$ is assumed to have the form

$$R(z) = A \exp[-az], \quad (13)$$

so that

$$V = \left[\frac{A}{a} \right] \exp[-as]. \quad (14)$$

The prefactor A is the neutralization rate at the image plane, and $(1/a)$ is the decay length for the neutralization rate. There is no unique solution to Eq. (14) for a and A . Values of a in the range $2\text{--}5 \text{ \AA}^{-1}$ are reported by Hagstrum to correspond to values of A between 7.1×10^{16} and $2.5 \times 10^{22} \text{ s}^{-1}$, for the neutralization of noble gas ions near a metal surface.³ For comparison, in this study, with $V = 1.04 \times 10^6$ m/s and $s \sim 1 \text{ \AA}$, the same values for the parameter a correspond to A ranging from 1.5×10^{17} to $7.7 \times 10^{18} \text{ s}^{-1}$, which are consistent with Hagstrum's results. This range of values determined for A depends on the parameters chosen to model the initial IEAD, in Eq. (7). However, uncertainties in these parameters appear to have only a minor effect on A . When variations in the values chosen for \bar{E}_0 , ΔE_0 , $\Delta\theta_0$, and W were tried (never exceeding physically realistic limits), it was found that even the largest deviations from the best-fit values change A by no more than a factor of 10, and typically by much less.

IV. DISCUSSION

With the effects of surface work-function variations, image-charge interactions, and neutralization accounted for, a few conclusions can be made. For example, Fig. 3 shows that the Cl^+ ESDIAD pattern is sharply peaked toward normal. This is consistent with Cl^+ emission from SiCl surface species, which are expected to have Si—Cl bonds oriented along the surface normal direction. Yet, in addition to SiCl, higher chlorides are also known to exist on the surface, based on the results of Si 2*p* photoelectron spectroscopy carried out on Si(111)-7×7 wafers exposed to Cl_2 , which show that both SiCl_2 and SiCl_3 form at Cl coverages below that used to generate the data shown in Fig. 3.⁸ If the bonds in the SiCl_2 and SiCl_3 species are nearly tetragonal, and a crystalline substrate is assumed, the angles of Si—Cl bonds from the surface normal would be about 55° and 70° , respectively. Since the critical angle for desorption is much less than either of these, no Cl^+ from SiCl_2 or SiCl_3 is seen. If the Si—Cl bonds in these species were randomly oriented, however, possibly due to some reaction-induced surface disorder, a broad Cl^+ ESD angular distribution would be expected, but this is also not observed. This evidence does not rule out the stimulated desorption of neutral Cl from the higher chlorides, but it does indicate that, although higher chlorides reside on the surface, the observed Cl^+ emission arises only from SiCl species.

In contrast, in the case of Si(111) reacted with atomic F (via XeF_2), F^+ stimulated desorption intensity has been shown to originate from the higher fluoride species as well as from SiF.^{14,22,23} This was determined by a careful analysis of the F^+ photon-stimulated desorption (PSD) yield near the Si 2*p* absorption edge. Note that a similar analysis for $\text{Cl}_2/\text{Si}(111)\text{-}7\times 7$ cannot be made, however, because direct excitation of the Si 2*p* core level does not lead to Cl^+ desorption.⁴ There are several reasons why F^+ originates from the higher fluorides in F/Si, even though Cl^+ is not emitted from higher chlorides in Cl_2/Si . For example, a major difference between the F/Si and Cl_2/Si systems is the degree of surface disruption that results from the halogenation reaction. In general, the Cl_2/Si reaction quickly saturates, with between 1 and 2 ML of Cl adsorbed,^{4,8} whereas the reaction of Si with atomic F disrupts the surface and does not saturate,^{24–28} but instead results in continuous etching via the formation of volatile SiF_4 .²⁹ Because of this, SiF_x species are randomly oriented on the surface and therefore have many Si—F bonds in more favorable directions, i.e., with angles less than the critical angle for desorption. In addition, the v_0 term in the ion survival probability is greater for F^+ than for Cl^+ , as F^+ has a greater kinetic energy and a lower mass. Taking the mean measured kinetic energy of F^+ to be 2.2 eV,¹⁴ and using the value $W = 3.6$ eV determined here, an initial velocity of $v_0 = 7700$ m/s is found for F^+ ESD from Si(111). All other things held constant, this larger value for v_0 will act to decrease neutralization at off-normal angles. Furthermore, because of the higher kinetic energy of the F^+ ions, if W is assumed to be the same between the two systems, the critical angle for recapture will be greater. For the mean F^+ kinetic

energy ($\bar{E}_0 = 5.8$ eV) used in the above calculation of v_0 , the critical angle is 38° , which is 10° greater than the critical angle at the mean kinetic energy of Cl^+ . The combination of random bond directions, decreased off-normal neutralization, and a greater critical angle for recapture explains why F^+ -stimulated desorption originates from all of the SiF_x species.

As part of an ESDIAD study of $\text{Cl}_2/\text{Si}(100)$, an analysis similar to the one reported here was carried out by Gao *et al.*³⁰ Based on the results of computer simulations, they derived a mean Cl^+ kinetic energy of 1.1 eV, explaining the difference between it and the measured energy of ~ 0.3 eV as being due to the unknown work-function difference between the sample and the grids of their RFA ESDIAD system. In that study, similar assumptions were made, namely that an initial Gaussian distribution of ion energies and angles is reacted upon by image forces and neutralization to give the observed ESDIAD pattern and IKED. A Hagstrum-type neutralization was also assumed, taking the values of A and a to be $2.4 \times 10^{15} \text{ s}^{-1}$ and 3 \AA^{-1} , respectively. From their reported numbers, a value of $(V/v_0) = 0.13$ is obtained. Such a small value of (V/v_0) corresponds to a much weaker angular dependence for neutralization than was found in the present study. Also, in that work, a critical angle for recapture of 39° is reported for ions desorbing with a mean initial kinetic energy of 2.8 eV, implying an initial image-charge interaction strength W of only 1.7 eV. The differences in the value of W between that study and this one can be traced to the choice of location for the image plane. Gao *et al.* chose to place the image plane level with the topmost layer of Si atoms, whereas in the present study the image plane was positioned approximately halfway between the topmost Si atoms and the Cl adatoms. Finally, in that study, the initial bond angle for SiCl species on a chlorinated Si(100) surface was reported

to be $25^\circ \pm 4^\circ$. That angle was calculated from a zero-bias emission angle of 27° . If, instead of placing it at the level of the topmost Si atoms, the image plane is assumed to be at the height found in this study (about 1.2 Å above the Si atoms), then a 27° emission angle is found to correspond to a bond angle of only $\sim 12^\circ$. In fact, depending on how the calculations are done and on the value of the zero-bias Cl^+ emission angle chosen,^{11,30} an initial bond angle in the range of $16^\circ \pm 4^\circ$ is found using the theory reported here.

V. SUMMARY

Cl^+ ESD ion energy and angular distributions were collected from $\text{Cl}_2/\text{Si}(111)-7 \times 7$. The work function of the surface is found to increase with Cl coverage, in a manner consistent with the buildup of screened Si-Cl dipoles on the surface. Shifts in the Cl^+ IKED are shown to correlate with changes in the work function. It is found that the angular distribution of Cl^+ ions is peaked sharply in the normal direction, with a FWHM of 19° , corresponding to Cl^+ emission originating only from SiCl species. Cl^+ IKED's were collected as a function of angle and were fit to model line shapes. From the fits, a set of parameters for the strength of the image-charge interaction and the angular dependence of neutralization are determined. This method for relating the motion of an ion near a surface to the motion of an ion measured far from the surface is easily generalized to other studies of ion-surface interactions.

ACKNOWLEDGMENTS

This work was supported by the Director, Office of Energy Research, Office of Basic Energy Sciences, Materials Sciences Division of the U.S. Department of Energy under Contract No. DE-AC03-76SF00098.

*Author to whom correspondence should be addressed.

¹Z. Miskovic, J. Vukanic, and T. E. Madey, *Surf. Sci.* **141**, 285 (1984).

²Z. Miskovic, J. Vukanic, and T. E. Madey, *Surf. Sci.* **169**, 405 (1986).

³H. D. Hagstrum, *Phys. Rev.* **96**, 336 (1954).

⁴T. D. Durbin, W. C. Simpson, V. Chakarian, D. K. Shuh, P. R. Varekamp, C. W. Lo, and J. A. Yarmoff, *Surf. Sci.* **316**, 257 (1994).

⁵Q. Guo, D. Sterratt, and E. M. Williams, Q. Guo, D. Sterratt, and E. M. Williams, *J. Electron Spectrosc. Relat. Phenom.* **72**, 31 (1995).

⁶D. Purdie, C. A. Muryn, N. S. Prakash, P. L. Wincott, G. Thornton, and D. S.-L. Law, *Surf. Sci.* **251/252**, 546 (1991).

⁷N. D. Spencer, P. J. Goddard, P. W. Davies, M. Kitson, and R. M. Lambert, *J. Vac. Sci. Technol. A* **1**, 1554 (1983).

⁸L. J. Whitman, S. A. Joyce, J. A. Yarmoff, F. R. McFeely, and L. J. Terminello, *Surf. Sci.* **232**, 297 (1990).

⁹T. E. Madey, *Science* **234**, 316 (1986).

¹⁰J. T. Yates, Jr., M. D. Alvey, M. J. Dresser, M. A. Henderson, M. Kiskinova, R. D. Ramsier, and A. Szabó, *Science* **255**, 1397 (1992).

¹¹S. L. Bennett, C. L. Greenwood, and E. M. Williams, *Surf.*

Sci. **290**, 267 (1993).

¹²M. J. Bozack, M. J. Dresser, W. J. Choyke, P. A. Taylor, and J. T. Yates, Jr., *Surf. Sci.* **184**, L332 (1987).

¹³T. E. Madey, R. Stockbauer, J. F. van der Veen, and D. E. Eastman, *Phys. Rev. Lett.* **45**, 187 (1980).

¹⁴J. A. Yarmoff and S. A. Joyce, *Phys. Rev. B* **40**, 3143 (1989).

¹⁵G. Dujardin, L. Hellner, L. Philippe, M.-J. Besnard-Ramage, and P. Cirkel, *Phys. Rev. B* **48**, 14 529 (1993).

¹⁶H. Luth, *Surfaces and Interfaces of Solids* (Springer-Verlag, Berlin, 1993), Vol. 15, p. 440.

¹⁷R. C. Weast, *Handbook of Chemistry and Physics* (Chemical Rubber, Cleveland, 1972).

¹⁸W. L. Clinton, *Phys. Rev. Lett.* **39**, 965 (1977).

¹⁹W. L. Clinton, *Surf. Sci.* **112**, L791 (1981).

²⁰J. D. Jackson, *Classical Electrodynamics* (Wiley, New York, 1962).

²¹D. Purdie, N. S. Prakash, K. G. Purcell, P. L. Wincott, and G. Thornton, *Phys. Rev. B* **48**, 2275 (1993).

²²J. A. Yarmoff, A. Taleb-Ibrahimi, F. R. McFeely, and P. Avouris, *Phys. Rev. Lett.* **60**, 960 (1988).

²³J. A. Yarmoff and S. A. Joyce, in *Synchrotron Radiation in Materials Research*, edited by J. H. Weaver, J. Gland, and R. Clarke (Materials Research Society, Pittsburgh, PA, 1989), p.

- 91.
- ²⁴C. W. Lo, P. R. Varekamp, D. K. Shuh, T. D. Durbin, V. Chakarian, and J. A. Yarmoff, *Surf. Sci.* **292**, 171 (1993).
- ²⁵C. W. Lo, D. K. Shuh, V. Chakarian, T. D. Durbin, P. R. Varekamp, and J. A. Yarmoff, *Phys. Rev. B* **47**, 15 648 (1993).
- ²⁶P. C. Weakliem, C. J. Wu, and E. A. Carter, *Phys. Rev. Lett.* **69**, 200 (1992).
- ²⁷P. C. Weakliem and E. A. Carter, *J. Chem. Phys.* **98**, 737 (1993).
- ²⁸C. J. Wu and E. A. Carter, *J. Am. Chem. Soc.* **113**, 9061 (1991).
- ²⁹H. F. Winters and F. A. Houle, *J. Appl. Phys.* **54**, 1218 (1983).
- ³⁰Q. Gao, C. C. Cheng, P. J. Chen, W. J. Choyke, and J. T. Yates, Jr., *J. Chem. Phys.* **98**, 8308 (1993).